PAPER • OPEN ACCESS

High-density amorphous ice: nucleation of nanosized low-density amorphous ice

To cite this article: Christina M Tonauer et al 2018 J. Phys.: Condens. Matter 30 034002

View the <u>article online</u> for updates and enhancements.



J. Phys.: Condens. Matter 30 (2018) 034002 (11pp)

High-density amorphous ice: nucleation of nanosized low-density amorphous ice

Christina M Tonauer[®], Markus Seidl-Nigsch¹[®] and Thomas Loerting[®]

Institute of Physical Chemistry, University of Innsbruck, Innrain 52c, 6020 Innsbruck, Austria

E-mail: thomas.loerting@uibk.ac.at

Received 29 September 2017, revised 22 November 2017 Accepted for publication 30 November 2017 Published 21 December 2017



Abstract

The pressure dependence of the crystallization temperature of different forms of expanded high-density amorphous ice (eHDA) was scrutinized. Crystallization at pressures 0.05-0.30 GPa was followed using volumetry and powder x-ray diffraction. eHDA samples were prepared via isothermal decompression of very high-density amorphous ice at 140 K to different end pressures between 0.07-0.30 GPa (eHDA^{0.07-0.3}). At 0.05-0.17 GPa the crystallization line $T_x(p)$ of all eHDA variants is the same. At pressures >0.17 GPa, all eHDA samples decompressed to pressures < 0.20 GPa exhibit significantly lower T_x values than eHDA^{0.2} and eHDA^{0.3}. We rationalize our findings with the presence of nanoscaled low-density amorphous ice (LDA) seeds that nucleate in eHDA when it is decompressed to pressures <0.20 GPa at 140 K. Below ~0.17 GPa, these nanosized LDA domains are latent within the HDA matrix, exhibiting no effect on T_x of eHDA $^{<0.2}$. Upon heating at pressures ≥0.17 GPa, these nanosized LDA nuclei transform to ice IX nuclei. They are favored sites for crystallization and, hence, lower T_x . By comparing crystallization experiments of bulk LDA with the ones involving nanosized LDA we are able to estimate the Laplace pressure and radius of ~0.3–0.8 nm for the nanodomains of LDA. The nucleation of LDA in eHDA revealed here is evidence for the first-order-like nature of the HDA \rightarrow LDA transition, supporting water's liquid-liquid transition scenarios.

Keywords: polyamorphism, ice, nucleation, crystallization

(Some figures may appear in colour only in the online journal)

1. Introduction

Since Mishima's discovery of water's polyamorphism [1, 2], a lot of experimental and computational effort has been made to gain deeper understanding of the nature of amorphous ices. Considering the densities at 77 K and ambient pressure, there are at least three amorphous states of water, low-density amorphous ice (LDA), high-density amorphous ice (HDA) and very high-density amorphous ice (VHDA) [1−4]. The reversible amorphous–amorphous transition between LDA ↔ HDA [5–7] seems to be quasi-first-order. This is

Original content from this work may be used under the terms of the Creative Commons Attribution 3.0 licence. Any further distribution of this work must maintain attribution to the author(s) and the title of the work, journal citation and DOI.

¹ Current address: Materials Development, Getzner Werkstoffe GmbH, Herrenau 5, 6706 Bürs, Austria.

consistent with several scenarios aimed at explaining water's anomalies, such as the singularity-free scenario [8], the critical point-free scenario [9] and the liquid-liquid critical point scenario (LLCP) proposed by Poole et al [10] (comprehensively reviewed in [11–13]). If the LDA \leftrightarrow HDA transition is indeed first-order, this would exclude the singularity-free scenario [14]. To distinguish between the LLCP scenario and the critical point-free scenario it would be necessary to measure thermodynamic response functions along the liquid-liquid transition line and to check whether singularities or extrema are encountered [15]. In the critical point-free scenario singularities are encountered at all positive pressures, whereas in the LLCP scenario extrema are encountered beyond the critical point. The experiments by Mishima on decompressioninduced melting of high pressure ices favor the LLCP scenario [16]. This scenario would explain the anomalous behavior of cold and supercooled water as a consequence of density and

entropy fluctuation at/near the proposed second critical point [11]. According to this hypothesis, stable and supercooled liquid water is a supercritical fluid of two states, low-density liquid (LDL) and high-density liquid (HDL), which are inseparable above the proposed second critical point [17]. Below the critical temperature, however, they would transform into each other discontinuously, involving a coexistence line (or related spinodal lines). The thermodynamics of such a two state model to understand water anomalies has very recently been described by Anisimov *et al* [18]. This interpretation also includes the assumption of LDA and HDA as vitrified forms of LDL and HDL, respectively.

Consequently, two distinct $T_g(p)$ lines representing the two different glass-to-liquid transitions are expected. This view is supported by computer simulations using the ST2 model [19] and experiments probing LDA's [20–23] and HDA's [24–32] glass-to-liquid transition utilizing differential scanning calorimetry, volumetry and dielectric relaxation spectroscopy at ambient and high pressure conditions. Hill et al applied small-angle neutron scattering to scrutinize structural changes in LDA upon slow heating [33]. Above 121 K, they could observe the onset of diffusive translational motion within the LDA sample, indicating a glass-to-liquid transition. Another recent study [34], using wide-angle x-ray scattering combined with x-ray photon-correlation spectroscopy, provides further evidence for the diffusive nature of molecular motions above the glass transition temperatures of both, LDA and HDA, supporting Poole's hypothesis [10]. Nevertheless, it is uncertain, whether the LLCP will ever be spotted directly or whether it will remain a virtual point in water's phase diagram, which can only be perceived from a distance [35].

The reason for this experimental inaccessibility of the p-T-region where the LLCP is expected (0.1 GPa, 220 K [36]; 0.027 GPa, 232 K [37]; 0.05 GPa, 223 K [38]; elaborately reviewed by Holten $et\ al\ [39]$) is the presence of fast crystallization kinetics within the borders of the homogeneous nucleation temperature $T_H(p)$ and the crystallization temperature of the amorphous ices $T_x(p)$. This p-T-region is often referred to as water's 'no man's land'. Note that the borders of this region are soft and highly dependent on the sample size and the experimental time scale [40].

Approaching the 'no man's land' from the amorphous ice states at the low temperature border, Seidl et al as well as Stern and Loerting could show the importance of appropriate sample pretreatment for shrinking water's 'no man's land' [41–43]. While Stern and Loerting scrutinized the crystallization behavior of VHDA and unannealed HDA (uHDA) in the intermediate pressure range 0.7–1.8 GPa [43], Seidl et al compared in their studies expanded HDA (eHDA) with uHDA concerning stability against crystallization and resulting crystallization products in the low pressure range 0.001-0.50 GPa [41, 42]. The term uHDA describes the type of HDA which was discovered by Mishima et al [1] when they compressed hexagonal ice (I_h) to 1.6 GPa at 77 K. It anneals to eHDA on warming below ~0.5 GPa [44] or via decompression of VHDA at 140 K [6]. The experimental strategy of Seidl et al is based on isobaric heating experiments and x-ray diffraction for characterization of the crystallization products. They observed that eHDA is more stable against crystallization than uHDA by up to 11 K. This discrepancy is especially pronounced at pressures ${<}0.20\,\mathrm{GPa}$. Additionally, the analysis of crystallization products revealed that at pressures ${<}0.20\,\mathrm{GPa}$ uHDA crystallizes always to a mixture of ice phases including ice I_h as the main share, whereas eHDA crystallizes to a single ice phase only. At pressures ranging from 0.30 GPa to 0.50 GPa, the qualitative difference between eHDA and uHDA considering the crystallization products disappears, while the lower crystallization temperature of uHDA compared to eHDA remains. Combining the results of their two studies [41, 42] Seidl et~al concluded:

- (i) At pressures $\leq 0.20\,\text{GPa}$ uHDA consists of an amorphous matrix with embedded nanocrystalline I_h domains ($<2\,\text{nm}$) triggering crystal growth of I_h when heated, whereas eHDA appears to be fully glassy and, thus, showing elevated crystallization temperatures.
- (ii) At higher pressures (0.30–0.50 GPa) nanocrystalline I_h domains in uHDA experience a polymorphic phase transition to ice IX. Again, the presence of nanoscaled ordered structures favor crystal growth upon heating, decreasing T_x with respect to eHDA.

These results favor the conjecture that eHDA, due to its apparent glassy nature, instead of uHDA, may be the low temperature proxy of the proposed HDL of water. Consequently, employing eHDA, as well as VHDA [43], could enable further exploration of (so far) inaccessible *p-T*-regions within water's phase diagram in order to gather further evidence for or against the proposed LLCP scenario [10].

In that context, the present study focuses on the aspect of preparation of eHDA. One main question is, whether eHDA, usually produced via decompression of VHDA at 140 K to an end pressure of 0.20 GPa [42], could become even more thermally stable against crystallization if it was prepared via decompression of VHDA to end pressures <0.20 GPa. Considering the phase diagram including (metastable) amorphous states in figure 1, the end pressure of decompression of VHDA (for preparation of eHDA) is limited by the spinodal of the HDA → LDA transition. The border between LDA and HDA was obtained by Mishima via decompression experiments of HDA at different temperatures [5]. Winkel et al conducted decompression experiments of VHDA in a pressure range 1.10-0.02 GPa at 140 K [6]. They located the quasi-discontinuous HDA → LDA transition at a pressure of ~0.06 GPa at 140 K. In the present study, this pressure is considered to be the ultimate limit of decompression for the preparation of eHDA. However, as we are going to show in the following, even at end pressures > 0.06 GPa and < 0.20 GPa, the vicinity to the HDA → LDA spinodal during the preparation of eHDA has a significant influence on the nature of eHDA.

2. Experimental

2.1. Apparatus

In the current study the same setup was used as it was employed by Seidl *et al* [41, 42]. More precisely, a custom-made

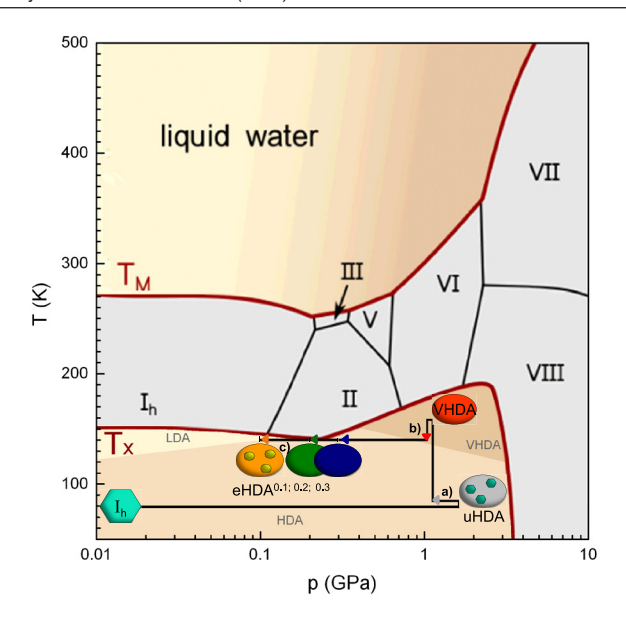


Figure 1. Phase diagram of water including the (metastable) amorphous ices LDA, HDA and VHDA, surrounded by the thick red crystallization line T_x . The thin line separating LDA and HDA was taken from figure 3 in [5], whereas the line between HDA and VHDA was deducted from figure 3(b) in [6]. Note that the HDA-LDA line represents a downstroke transition, whereas the HDA-VHDA line represents an upstroke transition—none is a binodal. Colored symbols and arrows represent the preparation route for eHDA, starting from hexagonal ice I_h (turquoise hexagon) via uHDA (grey ellipse with small hexagons, denoting remnants of I_h [41, 42]) and VHDA (red ellipse). Depending on the end pressure of the decompression VHDA → eHDA, eHDA is referred to as eHDA^{0.3} (blue), eHDA^{0.2} (green) and eHDA^{0.1} (orange with small yellow ellipses, denoting nanosized LDA domains). Adapted figure with permission from [40], Copyright 2016 by the American Physical Society.

high-pressure piston cylinder with a 8 mm bore together with a commercial 'universal material testing machine' (*Zwick*, model BZ100/TL3S) was utilized, for both, the high-pressure preparation of the sample as well as the subsequent *in situ* pressure dependent crystallization experiments. Temperature control was accomplished using a Pt-100 temperature sensor, which was inserted in the respective bore in the piston cylinder. This experimental setup enables the simultaneous detection and control of piston displacement (corresponding to volume change), temperature and pressure. For temperature control a *Lakeshore* temperature controller, operated via a self-written LABVIEW program was used. Control of piston displacement and pressure was accomplished using the commercial software TESTXPERT 7.1 (*Zwick*). For further details see [45].

2.2. Preparation of eHDA samples and in situ crystallization experiments

All ice samples in the present study were prepared by pipetting $300 \,\mu$ l of ultrapure liquid water into a precooled container made of ~0.3 g indium foil, a convenient low-temperature lubrication material preventing undesirable phase transitions in the sample due to shock-wave heating [1]. This effect can occur if a piston is stuck (due to friction within the bore) and

suddenly released by applying increased pressure leading to a quick heating and pressure-release event. Therefore, the use of indium as a lubricant is inevitable [1]. eHDA samples for subsequent crystallization experiments were prepared via the following steps (see figure 1).

2.2.a. Preparation of uHDA via isothermal compression of hexagonal ice I_h . In figure 1 this step is depicted by the horizontal arrow with a grey arrowhead. Hexagonal ice (big turquoise hexagon) is compressed from atmospheric pressure to 1.6 GPa. Following in essence the protocol by Mishima *et al* [1], subsequently, decompression to 1.1 GPa is performed ($T \sim 77 \, \text{K}$; compression/decompression rate: 0.1 GPa min⁻¹). This results in the amorphous matrix (grey ellipse) containing distorted I_h nanocrystallites [41, 42] (small turquoise hexagons in grey ellipse), see figure 1.

2.2.b. Preparation of VHDA via isobaric heating of uHDA. The vertical arrow with red arrowhead in figure 1 sketches the formation of VHDA: uHDA is isobarically heated from 77 K to $160 \, \text{K}$ and subsequently cooled to $140 \, \text{K}$ ($p=1.1 \, \text{GPa}$; heating/cooling rate: ~2 K min⁻¹), following the protocol by Loerting *et al* [3]. This step results in a denser amorphous matrix, essentially void of nanocrystalline domains [43], as indicated in figure 1 (red ellipse).

2.2.c. Preparation of eHDA via isothermal decompression of VHDA. In order to yield eHDA, we followed the protocol of Winkel et al [6]. VHDA is isothermally decompressed at 140 K to a certain end pressure between 0.07-0.30 GPa. The resulting different sorts of eHDA are referred to as eHDA^{0.07-0.3}, depending on the respective end pressure, stated as a superscript (in GPa). This preparation step is visualized in figure 1 by a horizontal arrow, directed to the left. Differently colored arrowheads correspond to the different sorts of eHDA resulting from different end pressures (eHDA^{0.3}: blue ellipse; eHDA^{0.2}: green ellipse; eHDA^{0.1}: orange ellipse with small yellow ellipses) ($T = 140 \,\mathrm{K}$; decompression rate: 0.02 GPa min⁻¹). The different sorts of eHDA differ in terms of their densities, i.e. eHDA^{0.3} is denser than eHDA^{0.1} [46]. Note that we assume the formation of nanosized LDA domains (small yellow ellipses) within eHDA^{0.1} during the preparation process. The decompression temperature for preparation of eHDA^{0.1} (140 K) is above both glass transition temperatures in the pressure range where the LDA nuclei form (0.20–0.10 GPa). In this pressure range the $T_{\rm g}$ for HDA is 134 K at 0.10 GPa and 139 K at 0.20 GPa [28] and the T_{g} for LDA is 132 K at 0.10 GPa and 127 K at 0.20 GPa [19]. In other words, at 140 K the amorphous samples are kept above their glass transition temperatures below 0.20 GPa. Considering the experimental conditions during the decompression of eHDA^{0.1}, an incipient transition HDA → LDA (or even HDL → LDL) seems plausible (see HDA → LDA spinodal in figure 1). This subject will be discussed in more detail on the basis of our experimental results below. After the preparation of an eHDA sample, the in situ crystallization experiments were conducted as follows.

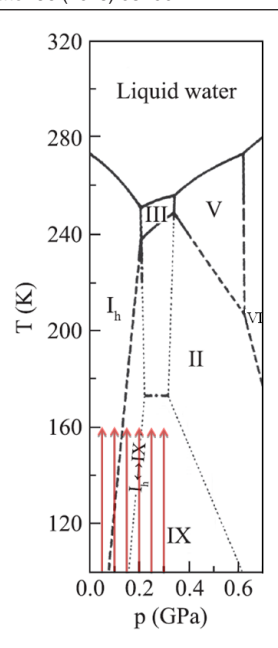


Figure 2. Phase diagram of water (phase boundaries from ref. [47]), including stable phases of water and metastable ice IX. Solid lines depict measured phase boundaries between stable phases, the dot-dashed line indicates the hydrogen-(dis)ordering temperature for the ice III → ice IX transition. Dashed lines depict estimated or extrapolated phase boundaries between stable phases, dotted lines indicate estimated or extrapolated borders between metastable phases. Red arrows represent isobaric heating experiments of eHDA in the current study. Adapted figure with permission from [42], Copyright 2015 by the American Physical Society.

2.2.d. Crystallization. The eHDA samples are then quenched to 77 K and (de)compressed to the desired pressure. Upon varying the pressure at 77 K the nature of the sample is retained, i.e. eHDA^{0.3} decompressed at 77 K to 0.10 GPa remains eHDA^{0.3} [6, 7].

The different sorts of ice are isobarically heated to temperatures $T_{\rm max} \ge 150\,\rm K$ (anyway, $T_{\rm max} > T_x$ or $T_{\rm trans}$) and subsequently cooled to 115 K (heating/cooling rate: ~2 K min^-1) and quenched to ~80 K by pouring liquid nitrogen around the piston cylinder. For eHDA, these *in situ* crystallization experiments were conducted at 6 different pressures ranging from 0.05–0.30 GPa. In figure 2, the isobaric heating experiments are sketched by light red arrows marked at every studied pressure in a phase diagram of water (including metastable ice IX). We note, e.g. eHDA^{0.3} slowly relaxes towards eHDA^{0.1} prior to crystallization upon heating at 0.10 GPa. That is, the superscript merely describes the sample history but does not indicate that eHDA^{0.3} is actually the state just before crystallization.

2.2.e. Second isobaric heating step to T_{max} . To check for complete transition, the sample was heated isobarically to T_{max} again at the same pressure as described in 2.2.d. applying a heating/cooling rate: ~2 K min⁻¹.

2.2.f. Quench recovery. After reaching T_{max} in 2.2.e, the sample was quenched to 77 K by pouring liquid nitrogen around

the piston cylinder and subsequently releasing the pressure ($T = 77 \,\mathrm{K}$; decompression rate: 0.02 GPa min⁻¹).

2.3. Preparation of bulk LDA and I_h samples for control experiments

As mentioned in section 2.2.c, we assume the formation of nanosized LDA nuclei in eHDA during the decompression of VHDA to pressures < 0.20 GPa at 140 K. The presence of these LDA nuclei influences the crystallization temperature of eHDA depending on the applied pressure during the crystallization experiment (see results in section 3). Therefore, we conducted control experiments on the pressure dependence of T_x in phase transitions in bulk LDA. Furthermore, bulk ice Ih samples were studied under pressure since we compare the phase transition temperatures obtained here with the ones obtained by Seidl et al on uHDA [41, 42]. Since these samples contain nanocrystalline domains of ice I_h, knowledge of the behavior of bulk ice I_h is needed for reference. (Bulk) LDA samples for the respective crystallization studies at pressures 0.20-0.40 GPa were obtained as described for eHDA in section 2.2, except for step 2.2.c, where VHDA was isothermally decompressed to 0.01 GPa in order to yield LDA [6]. Isobaric heating experiments at pressures 0.20-0.50 GPa, scrutinizing phase transitions in (bulk) ice I_h were done by isothermal (77 K) pre-compression of hexagonal ice to 0.70 GPa and decompression (0.1 GPa min⁻¹) to the desired pressure, followed by the steps described in sections 2.2.d–2.2.f.

2.4. Definition of crystallization temperature T_x

Volume change curves $\Delta V(T)$ are obtained by multiplication of the vertical (uniaxial) piston displacement with the bore's cross section (the temperature-dependence of the bore diameter (8 mm) was considered as insignificant). Usually, volume changes upon crystallization, and so it can be detected as a step in the $\Delta V(T)$ curves. To define the crystallization temperature T_x , the same method as in [42] was applied. Specifically, the intersection of a straight line through the mid-temperature part and a straight line through the high-temperature part of the step-like expansion (or contraction) in a $\Delta V(T)$ curve, representing the crystallization, was defined as T_x . In the case of a very rapid jump-like volume change at the transition, the temperature at the vertical edge was considered to be T_x . Note that the crystallization temperatures according to this definition have to be considered as end temperatures. Alternatively, also p(T) curves can be used for defining T_x . Although the heating experiments are conducted isobarically, fast expansions (contractions) at the transition cause temporary pressure deviations because the response of the apparatus is not fast enough. Consequently, the temperature at the maximum pressure deviation can be considered as T_x . However, in this study the T_x values were obtained by evaluation of the $\Delta V(T)$ curves to be able to compare our results with the results from Seidl et al [42].

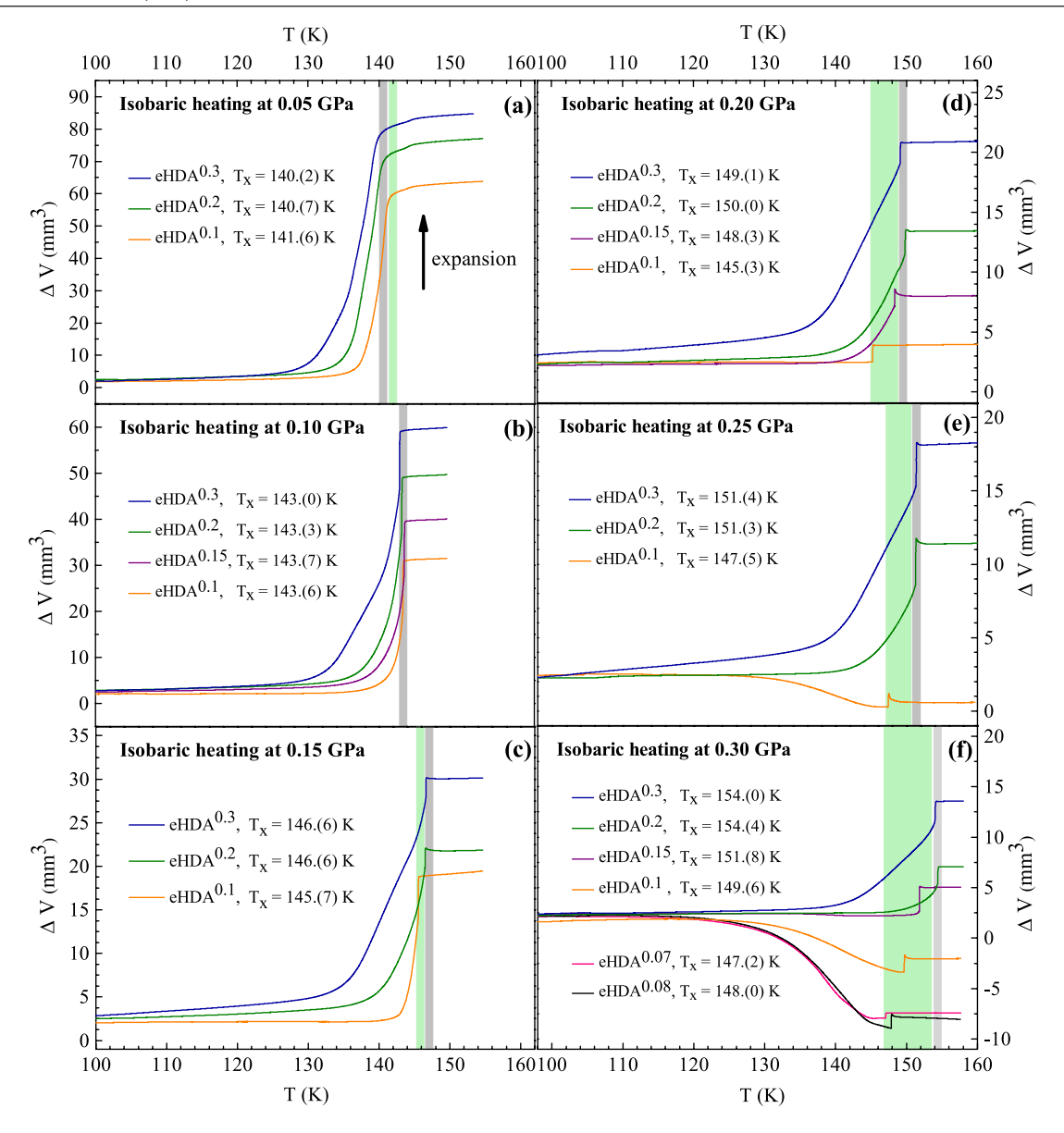


Figure 3. Volume curves $\Delta V(T)$ of crystallization experiments of eHDA at different pressures 0.05–0.30 GPa. (For experimental parameters, see section 2.2.d.). Subsequent isobaric cooling is not shown. T_x values for the crystallization experiments were obtained by the volume curves using the method explained in section 2.4. The grey bar is representing a temperature range of 1 K and marks the T_x range of eHDA^{0.2} and eHDA^{0.3}. The green bar indicates the T_x range of the remaining states of eHDA (eHDA^{0.07}; 0.08; 0.1; 0.15).

2.5. Apparatus correction

The piston displacement recorded by the machine does not only reflect the behavior of the ice samples but also contributions from the apparatus, especially the volume changes of the steel pistons. Hence, a correction of the volume curves was applied [42] utilizing isobaric heating experiments at four different pressures between 0.05–0.30 GPa, analogous to the step described in section 2.2.d, without ice samples, but with ~0.3 g indium foil. In good approximation, the resulting volume curves exhibit linear behavior. Therefore, straight lines were fit through the data points at temperatures ranging from 145–165 K. These linear functions were then subtracted from the raw $\Delta V(T)$ curves at each pressure (linear functions at intermediate pressures were obtained by linear interpolation). As a consequence, the volume curves shown in figure 3 only depict the behavior of the ice samples themselves.

2.6. Characterization of crystallization products

The quench-recovered samples were characterized using x-ray powder diffraction (Cu K α_1 radiation; diffractometer: Siemens D5000) in θ - θ geometry at ~80 K and subambient pressure (~10⁻³ bar). In order to conduct a qualitative analysis of the crystallization products of a sample, at least two x-ray diffractograms for each sample were considered. One prominent intensity maximum for each resulting crystalline ice phase was chosen (ice IX: at 29.6°, ice I_c : at 24.3°, ice V: at 30.9°). The intensities of these peak maxima were then summed up to a 'total intensity' for each diffractogram. The respective peak maximum intensities were then divided by the 'total intensity' in order to obtain polymorph fractions. Note that the stated percentage values are a rough approximation, because peak maximum intensities are not a direct measure of quantity of the present phases. Texture effects and different

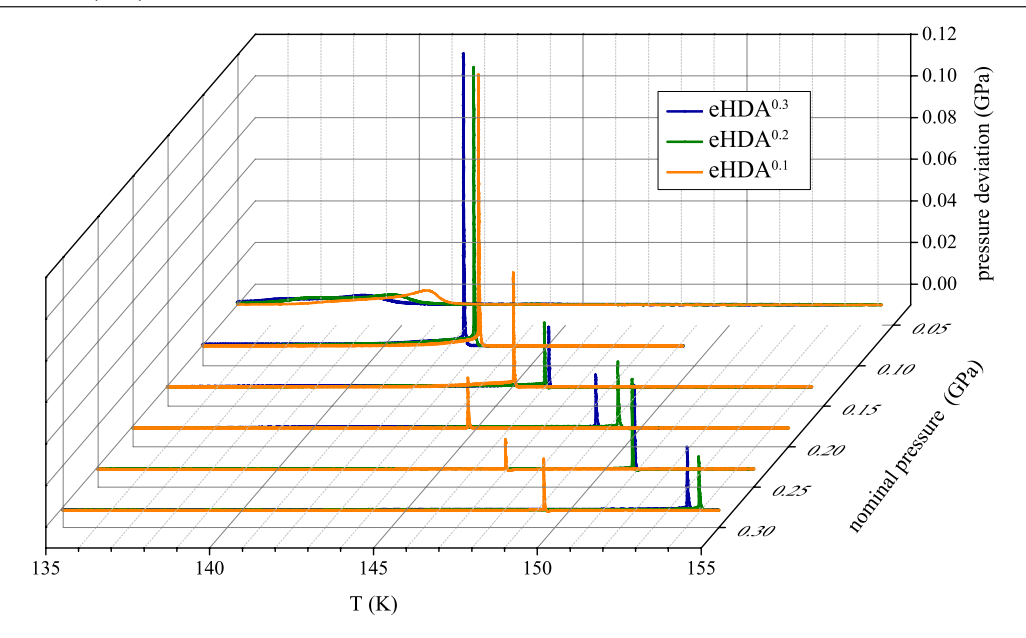


Figure 4. Pressure change $\Delta p(T, p)$ at the (formally) isobaric heating experiments causing crystallization of eHDA^{0.1; 0.2; 0.3}.

scattering cross sections for different polymorphs prevent a more accurate assessment.

3. Results

3.1. Volumetric crystallization study of eHDA

The volume curves $\Delta V(T)$ obtained from our crystallization experiments of eHDA at different pressures 0.05–0.30 GPa are depicted in figure 3. (For experimental parameters, see section 2.2.d). For clarity, the curves representing the subsequent isobaric cooling are omitted. T_x values for the crystallization experiments were obtained by the volume curves using the method explained in section 2.4. The grey bar in each $\Delta V(T)$ diagram is representing a temperature range of 1 K and marks the T_x range of eHDA^{0.2} and eHDA^{0.3}. That is, T_x for eHDA^{0.2} and eHDA^{0.3} are identical within the error bar of the method. The green bar indicates the T_x range of the remaining states of eHDA (eHDA^{0.07; 0.08; 0.1; 0.15}). Note that at 0.05 GPa (figure 3(a)) the green bar is at higher temperatures (~1 K) than the grey bar, at 0.10 GPa (figure 3(b)) both bars coincide within ~0.7 K and at higher pressures, see figures 3(c)–(f), the green bar broadens and is always at lower temperatures than the grey bar. That is, at pressures ≥ 0.15 GPa, T_x of eHDA $^{<0.2}$ is always lower than T_r of eHDA $^{>0.2}$. This effect becomes more prominent with increasing pressure. At 0.15 GPa (figure 3(c)) T_x of eHDA^{0.1} is only ~1 K lower than T_x of eHDA^{\geq 0.2}, whereas at 0.30 GPa (figure 3(f)) T_x of eHDA^{0.1} is ~5 K lower than T_x of eHDA^{≥0.2}.

In order to test whether decompression to lower pressures than 0.10 GPa during the preparation of eHDA could lower T_x even further (compared to eHDA $^{>0.2}$), eHDA $^{0.08}$ and eHDA $^{0.07}$ were prepared and isobarically heated at 0.30 GPa. As it is shown in figure 3(f), our assumption was confirmed by the experiments. T_x of eHDA $^{0.07}$ is ~7 K lower than T_x of eHDA $^{>0.2}$.

Crystallization events can also be monitored by the pressure change Δp (T, p) at the (formally) isobaric heating experiments (figure 4). For reasons of clarity, only the curves of eHDA^{0.1};0.2;0.3 are depicted. As already mentioned, the temperature at the maximum of pressure increase can also be used to define the crystallization temperature T_x . Figure 4 illustrates the crystallization behavior as mentioned above: at pressures 0.05–0.15 GPa the Δp -peaks of all three sorts of eHDA are aligned within a temperature interval of less than 1.5 K. Above 0.15 GPa, eHDA^{0.2} and eHDA^{0.3} remain aligned but the Δp -peaks of eHDA^{0.1} are shifted to significantly lower temperatures.

In figure 5, the T_x data collected from our isobaric heating experiments of eHDA are summarized: figure 5(a) depicts crystallization temperature as a function of pressure of eHDA^{0.07-} 0.3 as extracted from figure 3 in comparison with uHDA (adapted from [42]). For repeated experiments, error bars were calculated from the difference of the highest and the lowest measured value at a certain pressure. Crystallization experiments of eHDA decompressed to 0.07 and 0.08 GPa were only conducted at 0.30 GPa, to exhibit the large difference of ~7 K between T_x of eHDA^{0.2; 0.3} and eHDA decompressed to pressures as low as 0.07 GPa. While $T_x(p)$ is well described for eHDA $^{0.2}$ and eHDA $^{0.3}$ by a linear function this is not the case for eHDA^{0.1}. The kink of the $T_x(p)$ line of eHDA^{0.1} around ~0.17 GPa indicates a change in the crystallization process. A similar kink, but for the $T_x(p)$ line of uHDA, was observed at ~0.25 GPa by Seidl et al [41, 42]—see grey line in figure 5(a). They explained this effect with the presence of nanosized I_h crystallization seeds within the amorphous matrix of uHDA at <0.25 GPa. At pressures >0.25 GPa these nuclei transform to ice IX upon isobaric heating, decreasing the slope of the $T_x(p)$ line significantly. In figure 5(b), this phase transition, identified by Seidl et al [41, 42], is sketched by grey ellipses. Below 0.25 GPa the starting material of crystallization is uHDA with embedded I_h nuclei (small turquoise hexagons). Above 0.25 GPa the I_h nuclei have transformed to ice IX nuclei (small light blue squares). Figure 5(b) also contains a sketch of

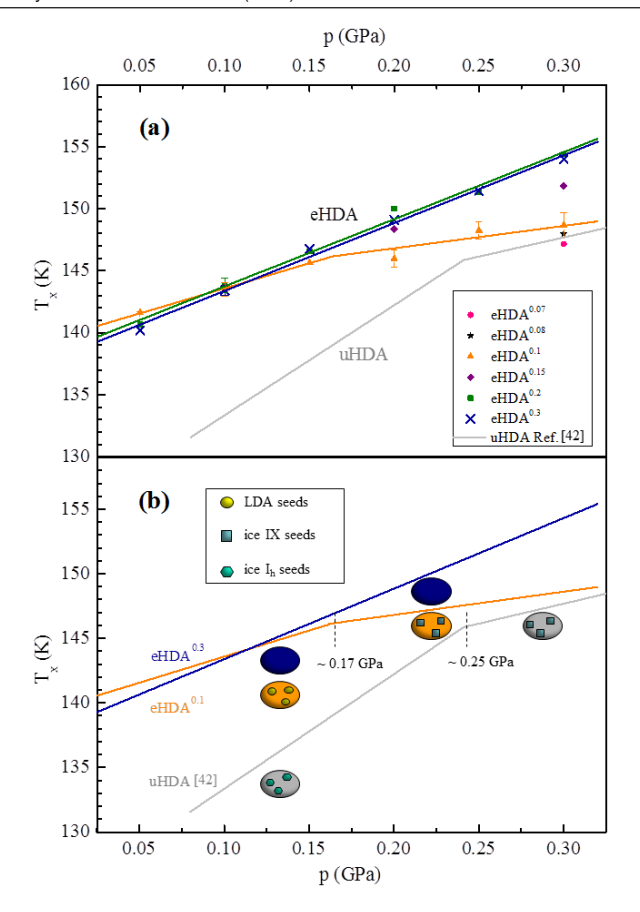


Figure 5. (a) Crystallization temperature as a function of pressure of eHDA $^{0.07-0.3}$ (current study) and uHDA. Adapted figure with permission from [42], Copyright 2015 by the American Physical Society. For eHDA $^{0.1; 0.2; 0.3}$ straight lines were fit through the data points. If applicable, error bars were calculated from the difference of the highest and the lowest measured value at a certain pressure. Crystallization experiments of eHDA decompressed to 0.07 and 0.08 GPa were only conducted at 0.30 GPa. (b) Crystallization temperature as a function of pressure, shown only for eHDA $^{0.3}$, eHDA $^{0.1}$ and uHDA [42] for clarity. The microscopic picture we could derive from our experimental results is represented by the sketch. eHDA $^{0.1}$ contains nanosized LDA seeds that transform to ice IX seeds above ~0.17 GPa. uHDA contains ice I_h seeds that transform to ice IX seeds above ~0.25 GPa. By contrast, eHDA $^{0.3}$ exhibits a linear $T_x(p)$ line throughout the studied pressure range, confirming its glassy nature.

the microscopic picture of eHDA^{0.1} and eHDA^{0.3} derived from the results of the present study. Our interpretation, including the phase transition of nanoscaled seeds of LDA to seeds of ice IX in eHDA^{0.1}, will be presented in detail in section 4.

3.2. XRD study of crystallization products of eHDA

A series of x-ray diffractograms is shown in figure 6(a). They were obtained for crystallized samples after isobaric heating at different pressures. The intensities are normalized to the highest peak in the respective diffractogram, resulting in 'relative intensity'. Peaks of high intensity indicating ice phases $(I_{c/h}, IX, V)$ are marked with roman numerals.

Based on the crystallization products, the studied pressure range (0.05–0.30 GPa) can be divided into three areas

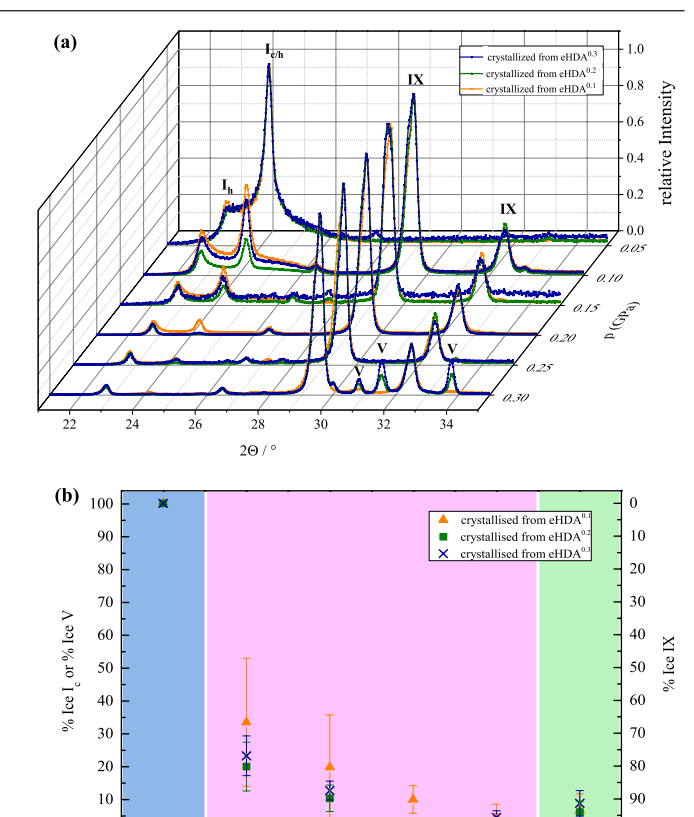


Figure 6. (a) Series of x-ray diffractograms measured of crystallized samples after isobaric heating at different pressures. Important Bragg peaks are marked with roman numerals indicating the ice phase. (b) Quantification of crystallization products of starting material eHDA $^{0.1;0.2;0.3}$. Peak maximum intensities at 29.6° (denoting ice IX), at 24.3° (denoting ice I $_c$) and 30.9° (denoting ice V) were considered for the analysis (see section 2.6).

0.15

0.05

0.10

0.25

0.20

p (GPa)

0.30

(see figure 6(b)). At 0.05 GPa, all studied sorts of eHDA (eHDA $^{0.1;\ 0.2;\ 0.3}$) crystallize to cubic ice, nowadays known as stacking-disordered ice I [48–51] (blue area). At pressures 0.10–0.25 GPa, mixtures of IX/I_c occur upon isobaric heating (pink area). The amount of I_c decreases with increasing pressure. At 0.30 GPa (green area), mixtures of IX/V emerge. The values of '% Ice I_c'/'% Ice IX' given in figure 6(b) are approximations, as described in section 2.6. However, relative changes of fractions with pressure are significant and valid. Thus, our method provides comprehensible insight into the three different crystallization modes that can be observed within the studied pressure range.

Figure 7 summarizes the results of the volumetric studies and the x-ray diffraction studies on eHDA^{0.1}, eHDA^{0.3} (present study) and uHDA [41, 42] at 0.10 GPa and 0.30 GPa. The amorphous starting materials are sketched as ellipses, representing the microscopic picture of eHDA^{0.1} derived from our results (section 4) and uHDA [41, 42]. T_x for each amorphous material and pressure is marked as a horizontal line. The crystallization products (main component written first) are given above T_x . Note, T_x of uHDA at 0.10 GPa is considerably lower than T_x of eHDA^{0.1}, which is similar to T_x of eHDA^{0.3}. At 0.30 GPa, however, T_x of uHDA is similar

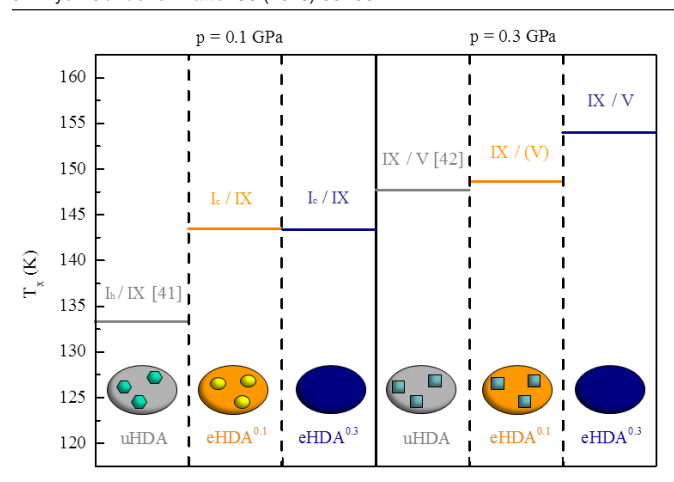


Figure 7. Sketch of transformations that take place upon heating at $0.10\,\mathrm{GPa}$ (left) and $0.30\,\mathrm{GPa}$ (right). Crystallization temperature T_x is depicted as horizontal line. Below the horizontal line, the amorphous samples are represented by ellipses (at $0.10\,\mathrm{GPa}$: uHDA with remnants of hexagonal ice [41]; eHDA^{0.1} with nanoscaled LDA domains, subject of the current study; eHDA^{0.3} as apparently fully amorphous; at $0.30\,\mathrm{GPa}$: uHDA after transformation of I_h seeds to ice IX seeds; eHDA^{0.1} after transformation of LDA seeds to ice IX seeds; eHDA^{0.3} remaining fully amorphous). Above the horizontal line, the resulting crystallization products are listed (main component listed first).

to T_x eHDA^{0.1} but significantly lower than T_x of eHDA^{0.3}. That is, nanosized LDA domains in eHDA^{0.1} at 0.10 GPa do not influence the crystallization temperature, whereas ice I_h nuclei in uHDA do [41, 42]. Furthermore, ice IX nuclei lower T_x both for eHDA^{0.1} and uHDA compared to eHDA^{0.3}. To answer the question, why nanoscaled LDA nuclei do not lower T_x of eHDA^{0.1}, crystallization studies of bulk LDA were conducted.

3.3. Crystallization/polymorphic transition of (bulk) LDA/Ih

Similar to the experiments scrutinizing eHDA, isobaric heating experiments and subsequent characterization by use of x-ray diffraction were done for bulk LDA and bulk I_h. Crystallization temperatures T_x (transformation temperatures T_{trans}) of LDA (I_h) were obtained from the respective $\Delta V(T)$ curves, as described in section 2.4. Figure 8 depicts the results of the crystallization experiments and the XRD measurements. T_x (yellow) and T_{trans} (turquoise) as a function of pressure for bulk LDA and bulk ice I_h are shown. Additionally, the starting materials and resulting crystallization products are depicted by the respective symbols. The vertical dashed lines crossing $T_x(p)$ and $T_{trans}(p)$ indicate a change in the mechanism of the respective phase transition. Below ~0.37 GPa LDA (yellow ellipse) crystallizes to cubic ice I_c (azure cube) upon heating, above ~0.37 GPa LDA crystallizes to ice IX (light blue square). Below ~0.45 GPa I_h transforms to ice II (purple triangle) upon heating, above ~0.45 GPa I_h transforms to ice IX (see phase diagram in figure 2). That is, the crystallization mechanism changes at ~0.37 GPa for bulk LDA, and at ~0.17 GPa for nanocrystalline LDA (kink for eHDA^{0.1} in figures 5(a) and (b)). Similarly, the transformation mechanism for I_h changes at ~0.45 GPa in the bulk, and at \sim 0.25 GPa in nanocrystalline I_h (kink for uHDA in figures 5(a)

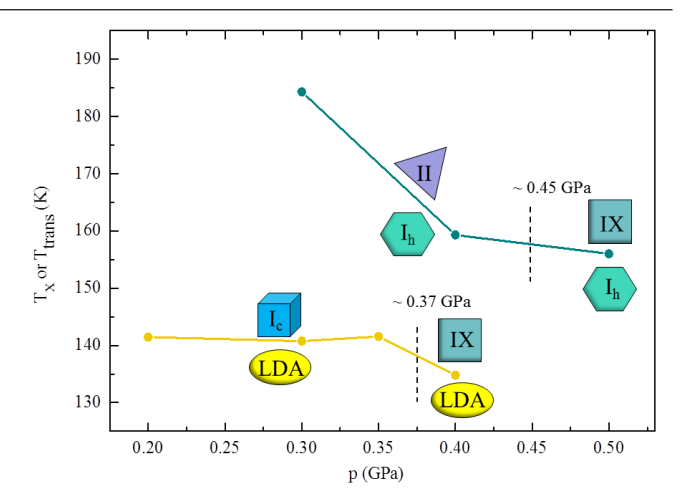


Figure 8. Transition temperature T_{trans} (turquoise) and crystallization temperature T_x (yellow) as a function of pressure for bulk ice I_h and bulk LDA, respectively. Sketch of involved phases/amorphous states. The vertical dashed lines indicate a change in the transformation mechanism.

and (b)). In both cases there is a downshift of ~0.20 GPa when comparing the change of mechanism in nanoscaled seeds with the bulk material.

4. Discussion

4.1. Crystallization of eHDA

Based on the crystallization line $T_x(p)$ of eHDA^{0.2} and eHDA^{0.3} in figure 5(a), as well as the analysis of the resulting crystallization products in figure 6(b), we conclude that there is no significant difference between the nature of eHDA^{0.2} and eHDA^{0.3}, neither in the thermal stability against crystallization nor in the crystallization mode, as both starting materials yield similar crystallization products. The presence of one main crystalline phase (and only marginal amounts of another phase) after crystallization indicates that both, eHDA^{0.2} and eHDA^{0.3}, can be regarded glassy, in other words the low-temperature proxy of HDL [28, 31, 42]. By contrast, the crystallization line $T_x(p)$ of eHDA^{0.1} exhibits quite different behavior (see figure 5(a)). The measured T_x values at pressures 0.05, 0.10 and 0.15 GPa can be connected by a straight line, whereas the data points from 0.20, 0.25 and 0.30 GPa can be connected by another straight line of decreased slope. Between 0.15 GPa and 0.20 GPa (in our diagram shown at ~0.17 GPa) eHDA^{0.1} seems to change in a way that causes a significant effect on the crystallization behavior. Below ~0.17 GPa the $T_x(p)$ line of eHDA^{0.1} exhibits a similar slope as the respective slopes of eHDA^{0.2, 0.3}, but at pressures above ~0.17 GPa eHDA^{0.1} shows significantly decreased thermal stability against crystallization by up to ~7 K. Apparently, crystallization kinetics in eHDA^{0.1} seem to be enhanced at pressures above ~0.17 GPa.

We interpret our results in the following way: during the preparation of eHDA^{0.1} (isothermal decompression of VHDA at 140 K, see section 2.2.c) domains of LDA nucleate upon decompression to 0.10 GPa within the eHDA matrix. eHDA^{0.1} is decompressed well beyond the HDA-LDA binodal located

at \sim 0.2 GPa [52] and close to the spinodal [5] shown in figure 1. This corresponds to the p-T regime, in which LDA is thermodynamically favored over HDA and, hence, nucleation is possible. At 140 K the rate of nucleation is sufficiently high to form a significant amount of nuclei larger than the critical radius at the time scale of minutes. However, at 140 K the rate of growth is still too low for significant growth of the nuclei in our experiments. Close to the spinodal the size of the critical cluster is rather small, probably just a few molecules of water [53], so that the critical cluster size can be exceeded easily in spite of slow kinetics.

As the LDA domains remain hidden in x-ray diffractograms (see [6]), we conclude, that these domains have to be nanoscaled. In our experimental setup the size limit for the detection of ice crystals is on the order of $10 \,\mathrm{nm}$ as estimated based on the Debye–Scherrer equation considering the instrumental broadening and the signal to noise ratio for our typical measurements of $45 \,\mathrm{min}$. For crystallization experiments in the pressure range 0.05– $0.15 \,\mathrm{GPa}$ these LDA nuclei remain latent, showing no effect on the crystallization behavior compared to eHDA^{0.2; 0.3}. This is because T_x of LDA is ~140 K at 0.25– $0.35 \,\mathrm{GPa}$ (see figure 8, considering $0.20 \,\mathrm{GPa}$ internal pressure of the LDA nanodomains as demonstrated below), and hence about the same as T_x of eHDA. In other words, the presence of LDA domains does not enhance crystallization kinetics.

This observation changes at pressures ≥0.20 GPa. At higher pressures we witness a significant decrease of T_x for eHDA^{0.1}. We suggest a phase transition of the nanoscaled LDA nuclei to crystalline nuclei, which act as favored sites for crystal growth and thereby decreasing T_x of eHDA^{0.1}. Considering the crystallization products of eHDA^{0.1} (which do not differ significantly from the crystallization products of eHDA^{0.2, 0.3}, see figure 6(b)) we suggest, that LDA seeds transform to ice IX seeds. This observation resembles the one of Seidl et al [42], see figure 5(b). In their study, they proposed a phase transition of nanosized I_h seeds (remnants after pressure induced amorphization at 77 K [1]) in uHDA to ice IX seeds. At pressures $\leq 0.25 \,\mathrm{GPa}\ T_x$ for uHDA is up to 11 K lower than T_x of eHDA^{0.2} due to the presence of nanosized Ih seeds. This effect diminishes after transformation of the I_h nuclei to ice IX nuclei. At 0.30 GPa uHDA, eHDA $^{0.1}$, eHDA $^{0.08}$ and eHDA $^{0.07}$ crystallize at 147 \pm 1 K, and hence roughly 7 K lower than eHDA^{0.2} and eHDA^{0.3} (see figure 5(a)). The equality of T_x of uHDA and T_x of eHDA^{0.07–0.1} at 0.30 GPa shows that in both cases the same crystallization mechanism is operative, namely growth of ice IX domains. Despite the different preparation history, at 0.30 GPa and just below T_x , we consider uHDA and eHDA^{0.07–0.1} to be identical. By contrast, for eHDA^{0.2–0.3} the crystallization mechanism is different, namely crystallization of a homogeneous glassy matrix takes place in this case.

4.2. Comparison of phase transitions in the bulk and in nanosized nuclei

We scrutinized the phase transitions occurring in (bulk) LDA and (bulk) I_h upon isobaric heating. In figure 8 we summarize

our results: The T_x line of LDA shows almost no pressure dependence at pressures 0.20–0.35 GPa ($T_x \sim 140 \, \text{K}$). In this pressure range the resulting crystalline product is I_c with marginal amounts of ice IX. The ratio of crystalline products reverses at pressures higher than 0.35 GPa, showing ice IX as main product as well as marginal amounts of I_c .

Therefore, we estimate the minimal pressure for the transition of (bulk) LDA to (bulk) ice IX to be ~0.37 GPa upon heating. In comparison with eHDA $^{0.1}$, we experience this transition of nanoscaled LDA seeds to ice IX seeds at a minimal pressure of ~0.17 GPa (see kink for eHDA $^{0.1}$ in figure 5(a)). Considering the lowest pressure necessary for the transition LDA \rightarrow IX upon heating, there is a difference of about 0.20 GPa between (bulk) LDA and nanosized LDA domains in eHDA $^{0.1}$.

Comparing the change of transition mechanism in (bulk) ice I_h and nanosized I_h nuclei embedded in uHDA, there is also a difference of ~0.20 GPa observable. 0.45 GPa (vertical dashed line in figure 8) appears to be the minimum pressure necessary for the transition $I_h \rightarrow IX$ to happen in the bulk I_h system upon heating. The corresponding transition of I_h nanocrystallites in uHDA occurs at a minimal pressure of ~0.25 GPa [42] (see kink for uHDA in figure 5).

Summarizing the observation in bulk LDA and bulk I_h : The proposed phase transitions on the nanometer scale within eHDA $^{0.1}$ (LDA \rightarrow IX) and uHDA ($I_h \rightarrow$ IX) could also be observed in the respective macroscopic systems. Nevertheless, the transitions were only observable at pressures at least \sim 0.20 GPa higher than the pressure at the kink in the T_x line of eHDA $^{0.1}$ and uHDA, respectively. This pressure gap between the transitions in the bulk and in nanoscale can be explained by the high internal pressure within a nanosized nucleus, which has to compensate the external pressure and the surface tension of the nucleus. In this context, the Laplace equation ($\Delta p = 2 \sigma r^{-1}$; quantifying the difference between the internal pressure (in a curved object) and the external pressure Δp , Laplace pressure) was used to estimate the dimension of a LDA or I_h seed.

Therefore, Δp was assumed to be the pressure gap of ~0.20 GPa. A lower limit for the surface tension σ of LDA (or Ih) nuclei within a HDA matrix was taken from [53]. Espinosa et al calculated a surface tension of 29.8 mJ m⁻² for I_h nuclei within liquid water using the TIP4P/Ice model [53]. Based on the Laplace equation, the radius of a (spherical) LDA/I_h seed within eHDA^{0.1}/uHDA has then to be 0.3 nm. Note, this is just a rough approximation. Instead of an ice I_h seed in liquid water, in our case we actually have an LDA seed in HDA, or ultraviscous HDL [19, 28]. Therefore, an exact value for the surface tension is unknown. As an upper limit we tentatively assume a surface tension of 75 mJ m⁻², corresponding to the liquid vapor surface tension at 273 K [54, 55]. The true surface tension of LDA within HDA is presumably clearly lower than this value. Under this premise a nucleus radius of 0.8 nm results. Assuming a spherical seed, it then contains ~100-200 water molecules.

The result shows a reasonable order of magnitude for the size of a single seed, another indirect hint for our proposed microscopic picture of eHDA^{0.1}.

5. Conclusions

We have conducted a study on the pressure dependence of the crystallization temperature in eHDA samples of different preparation history. We conclude that the crystallization temperatures summarized in figure 5(b) show that different crystallization modes are operative for different samples. We argue that the observations can only be rationalized on the basis of LDA-nanodomains forming in eHDA^{<0.2}. We rule out a crystalline nature of the nanodomains, e.g. ice I_h [41] or ice 0 [56], since crystalline domains would enhance crystallization at low pressures in contrast to our findings. Furthermore, these nanodomains transform to crystalline ice IX nanodomains above ~0.17 GPa. We want to emphasize the novelty as well as the exceptionality of our proposed microscopic picture describing the nature of eHDA^{0.1}. It involves the nucleation of nanoscaled amorphous seeds within another (highly dense) amorphous matrix. Our study uncovers the nucleation of LDA in eHDA upon decompression of VHDA to pressures <0.20 GPa. The nucleation of LDA in eHDA is another, yet unknown piece of evidence for the first-order nature of the HDA → LDA transition, supporting scenarios including a liquid–liquid transition [9, 10].

In fact, considering that $140 \, \text{K}$ is above the glass transition temperatures of both HDA and LDA, we actually interpret the observations on the basis of LDL nanodomains nucleating in HDL, i.e. one liquid nucleating in another. This interpretation requires that amorphous ices turn into ultraviscous liquids above T_g , which is contested. While we regard the samples to be in the ultraviscous state [33, 34] other researchers consider the sample to be glassy even above T_g [57, 58].

Furthermore, we want to emphasize the significance of our observation of the LDA -> IX transition within nanosized domains in eHDA $^{0.1}$, similar to the $I_h \rightarrow IX$ transition in uHDA observed by Seidl et al [42]. In the present study we can show the different behavior of nanoscaled LDA domains in eHDA^{0.1} compared to the behavior of nanoscaled Ih in uHDA [42], pointing out the different nature of LDA and I_h. Below ~0.17 GPa, LDA-nanodomains remain latent, whereas I_h nanodomains significantly lower T_x . However, above ~0.17 GPa these nanodomains transform to ice IX. These nanocrystallites enhance the crystallization kinetics, resulting in up to \sim 7 K lower T_x values compared to homogeneous eHDA $^{0.2}$. In contrast, I_h nanocrystallites in uHDA decrease T_x significantly (up to 11 K at \leq 0.25 GPa) compared to eHDA^{0.2}, also below 0.17 GPa. When I_h nanocrystallites transform to ice IX (above ~0.25 GPa), the effect diminishes. That is, ice I_h nanocrystallites and LDA nanodomains have opposite effects on the crystallization kinetics up to a pressure of ~0.30 GPa.

Finally, conducting isobaric heating experiments probing bulk LDA and bulk I_h enables us to estimate the size of the LDA/ice IX nuclei in eHDA^{0.1}. Due to the elevated internal pressure within the LDA nuclei in eHDA^{0.1}, the nanoscaled LDA \rightarrow IX transition takes place at lower pressures compared to the bulk. Employing the Laplace equation, we can estimate the radius of a (spherical) LDA/ I_h seed within an eHDA^{0.1}/ uHDA matrix to be ~0.3–0.8 nm.

Acknowledgments

We thank Josef Stern for experimental help in the initial stage of this work. Support by the Austrian Science Fund FWF (French-Austrian bilateral project no. I1392 and project no. P26040) is gratefully acknowledged.

ORCID iDs

Christina M Tonauer https://orcid.org/0000-0001-6859-5344 Markus Seidl-Nigsch https://orcid.org/0000-0003-4033-450X Thomas Loerting https://orcid.org/0000-0001-6694-3843

References

- [1] Mishima O, Calvert L D and Whalley E 1984 Nature 310 393
- [2] Mishima O, Calvert L D and Whalley E 1985 Nature 314 76
- [3] Loerting T, Salzmann C, Kohl I, Mayer E and Hallbrucker A 2001 Phys. Chem. Chem. Phys. 3 5355
- [4] Loerting T, Winkel K, Seidl M, Bauer M, Mitterdorfer C, Handle P H, Salzmann C G, Mayer E, Finney J L and Bowron D T 2011 Phys. Chem. Chem. Phys. 13 8783
- [5] Mishima O 1994 J. Chem. Phys. 100 5910
- [6] Winkel K, Elsaesser M S, Mayer E and Loerting T 2008 J. Chem. Phys. 128 044510
- [7] Winkel K, Mayer E and Loerting T 2011 J. Phys. Chem. B 115 14141
- [8] Sastry S, Debenedetti P G, Sciortino F and Stanley H E 1996 Phys. Rev. E 53 6144
- [9] Angell C A 2008 Science 319 582
- [10] Poole P H, Sciortino F, Essmann U and Stanley H E 1992 Nature 360 324
- [11] Debenedetti P G 2003 J. Phys.: Condens. Matter 15 R1669
- [12] Caupin F 2015 J. Non-Cryst. Solids 407 441
- [13] Gallo P et al 2016 Chem. Rev. 116 7463
- [14] Pallares G, El Mekki Azouzi M, Gonzalez M A, Aragones J L, Abascal J L F, Valeriani C and Caupin F 2014 Proc. Natl Acad. Sci. 111 7936
- [15] Holten V, Qiu C, Guillerm E, Wilke M, Rička J, Frenz M and Caupin F 2017 J. Phys. Chem. Lett. 8 5519
- [16] Mishima O 2000 Phys. Rev. Lett. 85 334
- [17] Russo J and Tanaka H 2014 Nat. Commun. 5 3556
- [18] Anisimov M A, Duška M, Caupin F, Amrhein L E, Rosenbaum A and Sadus R J 2017 arXiv:1708.03573
- [19] Giovambattista N, Loerting T, Lukanov B R and Starr F W 2012 Sci. Rep. 2 390
- [20] Johari G P, Hallbrucker A and Mayer E 1987 Nature 330 552
- [21] Kohl I, Bachmann L, Hallbrucker A, Mayer E and Loerting T 2005 Phys. Chem. Chem. Phys. 7 3210
- [22] Kohl I, Bachmann L, Mayer E, Hallbrucker A and Loerting T 2005 Nature 435 E1
- [23] Elsaesser M S, Winkel K, Mayer E and Loerting T 2010 Phys. Chem. Chem. Phys. 12 708
- [24] Mishima O 2004 J. Chem. Phys. 121 3161
- [25] Andersson O 2005 Phys. Rev. Lett. 95 205503
- [26] Andersson O and Inaba A 2006 Phys. Rev. B 74 184201
- [27] Andersson O 2008 J. Phys.: Condens. Matter 20 244115
- [28] Seidl M, Elsaesser M S, Winkel K, Zifferer G, Mayer E and Loerting T 2011 Phys. Rev. B 83 100201
- [29] Andersson O 2011 Proc. Natl Acad. Sci. 108 11013
- [30] Handle P H, Seidl M and Loerting T 2012 Phys. Rev. Lett. 108 225901
- [31] Amann-Winkel K, Gainaru C, Handle P H, Seidl M, Nelson N, Bohmer R and Loerting T 2013 Proc. Natl Acad. Sci. 110 17720

- [32] Loerting T, Fuentes-Landete V, Handle P H, Seidl M, Amann-Winkel K, Gainaru C and Boehmer R 2015 J. Non-Cryst. Solids 407 423
- [33] Hill C R, Mitterdorfer C, Youngs T G A, Bowron D T, Fraser H J and Loerting T 2016 *Phys. Rev. Lett.* **116** 215501
- [34] Perakis F et al 2017 Proc. Natl Acad. Sci. 114 8193
- [35] González M A, Valeriani C, Caupin F and Abascal J L F 2016 J. Chem. Phys. 145 054505
- [36] Mishima O and Stanley H E 1998 Nature 392 164
- [37] Fuentevilla D A and Anisimov M A 2006 Phys. Rev. Lett. 97 195702
- [38] Mishima O 2010 J. Chem. Phys. 133 144503
- [39] Holten V, Bertrand C E, Anisimov M A and Sengers J V 2012 J. Chem. Phys. 136 094507
- [40] Amann-Winkel K, Böhmer R, Fujara F, Gainaru C, Geil B and Loerting T 2016 Rev. Mod. Phys. 88 011002
- [41] Seidl M, Amann-Winkel K, Handle P H, Zifferer G and Loerting T 2013 Phys. Rev. B 88 174105
- [42] Seidl M, Fayter A, Stern J N, Zifferer G and Loerting T 2015 Phys. Rev. B 91 144201
- [43] Stern J and Loerting T 2017 Sci. Rep. 7 3995
- [44] Nelmes R J, Loveday J S, Strässle T, Bull C L, Guthrie M, Hamel G and Klotz S 2006 *Nat. Phys.* **2** 414
- [45] Seidl M, Fayter A, Stern J N, Amann-Winkel K, Bauer M and Loerting T 2015 Proc. of the 6th Zwick Academia

- Day 2015 (http://www.loerting.at/publications/seidl15-zwick.pdf)
- [46] Loerting T, Bauer M, Kohl I, Watschinger K, Winkel K and Mayer E 2011 J. Phys. Chem. B 115 14167
- [47] Hobbs P V 1974 Ice Physics (Oxford: Clarendon) p 61
- [48] Hansen T C, Koza M M and Kuhs W F 2008 J. Phys.: Condens. Matter 20 285104
- [49] Hansen T C, Koza M M, Lindner P and Kuhs W F 2008 J. Phys.: Condens. Matter 20 285105
- [50] Kuhs W F, Sippel C, Falenty A and Hansen T C 2012 Proc. Natl Acad. Sci. 109 21259
- [51] Malkin T L, Murray B J, Salzmann C G, Molinero V, Pickering S J and Whale T F 2015 Phys. Chem. Chem. Phys. 17 60
- [52] Whalley E, Klug D D and Handa Y P 1989 Nature 342 782
- [53] Espinosa J R, Vega C and Sanz E 2016 J. Phys. Chem. C 120 8068
- [54] IAPWS 2014 Revised Release on Surface Tension of Ordinary Water Substance R1-76 (http://www.iapws.org/relguide/ Surf-H2O.html)
- [55] Vega C and de Miguel E 2007 J. Chem. Phys. 126 154707
- [56] Russo J, Romano F and Tanaka H 2014 Nat. Mater. 13 733
- [57] Fisher M and Devlin J P 1995 J. Phys. Chem. 99 11584
- [58] Shephard J J and Salzmann C G 2016 J. Phys. Chem. Lett. 7 2281